

Proceedings of the Fifth Annual LHCP
ATL-PHYS-PROC-2017-XXX
October 29, 2021

ELECTROWEAK MEASUREMENTS AT THE LHC

ALEXANDER SAVIN

*On behalf of the ATLAS, LHCb and CMS Collaborations,
Department of Physics
University of Wisconsin-Madison, Madison, WI 53706-1390, USA*

ABSTRACT

A set of selected electroweak measurements from the LHC experiments is discussed. Results on forward-backward asymmetry in production of the Drell-Yan events in both dielectron and dimuon decay channels are presented together with results on the effective mixing angle measurements. Angular coefficients measured in the Z boson production are compared with theoretical predictions. Electroweak production of the vector bosons in association with two jets is presented.

PRESENTED AT

The Fifth Annual Conference
on Large Hadron Collider Physics
Shanghai Jiao Tong University, Shanghai, China
May 15-20, 2017

1 Introduction

The electroweak (EWK) measurements are playing an important role at the LHC. The measured cross sections allow better understanding of the standard model (SM) predictions and backgrounds to the searches beyond the SM. Recently available predictions at the next-to-next-to-leading order (NNLO) in QCD and next-to-leading order (NLO) in EWK require for comparisons high-precision measurements with well understood sources of the experimental and theoretical systematic uncertainties. The global SM parameters: vector boson masses, $\sin\theta_W$, α_{em} can also be measured thus providing important input to the models and global fits.

These proceedings cover only few selected EWK measurements performed by ATLAS [1], LHCb [2, 3], and CMS [4] collaborations. The measurements are related mainly to single vector boson production, more topics are discussed in other contributions that were presented at the same conference.

2 Forward-backward asymmetry in Drell-Yan production

The presence of both vector and axial-vector couplings of electroweak bosons to fermions lead to a forward-backward asymmetry A_{FB} in the production of Drell-Yan lepton pairs. The A_{FB} is defined as $A_{FB} = \frac{\sigma_F - \sigma_B}{\sigma_F + \sigma_B}$, where $\sigma_{F(B)}$ is the total cross section for the forward ($\cos\theta^* > 0$) and backward ($\cos\theta^* < 0$) events. To reduce the uncertainties due to the transverse momentum of the incoming quarks, the measurements use the Collins-Soper (CS) frame [5]. In the recent CMS measurement [6] at $\sqrt{s} = 8$ TeV the DY events were detected in decays to electron and muon pairs, with lepton transverse momentum, p_T , above 20 GeV and pseudorapidity $|\eta| < 2.4$ for muons, while for electrons the region was extended up to $|\eta| < 5$ by using forward hadron (HF) calorimeter for the electrons identification. The measurement is performed as a function of dilepton mass in bins of rapidity, y , of the dilepton system. Figure 1 shows the dilepton mass distributions for muon and electron decay channels, for events with $|y| < 2.4$. The extended region in y for electron pairs is shown in Fig. 2 (left). The data are well described by the simulation convoluted with data-driven background estimates. The backgrounds are relatively small. The major experimental uncertainties arise from the electron and muon energy corrections and from the unfolding procedure. The mass resolution in the forward region is not as good as in the central one, but this region is important since the ambiguity of the quark direction is lower at higher y and the dilution of A_{FB} is therefore smaller.

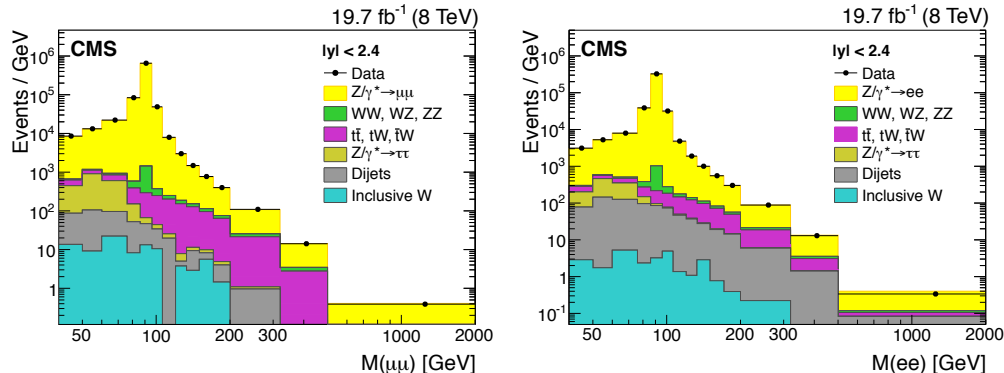


Figure 1: The dilepton reconstructed mass distributions for muon (left) and electron (right) decay channels, for events with $|y| < 2.4$ [6].

The A_{FB} measurement is performed as a function of dilepton mass in bins of rapidity. The shape of $\cos\theta_{CS}^*$ changes with the mass, one representative distribution for the dimuon channel for $\mu\mu$ mass range 133 – 150 GeV is shown in Fig. 2 (right). The stacked histograms represent the sum of the background contribution and signal. The data are well described by the expected distributions.

The combined dielectron and dimuon unfolded A_{FB} distributions in the central rapidity region $|y| < 1$

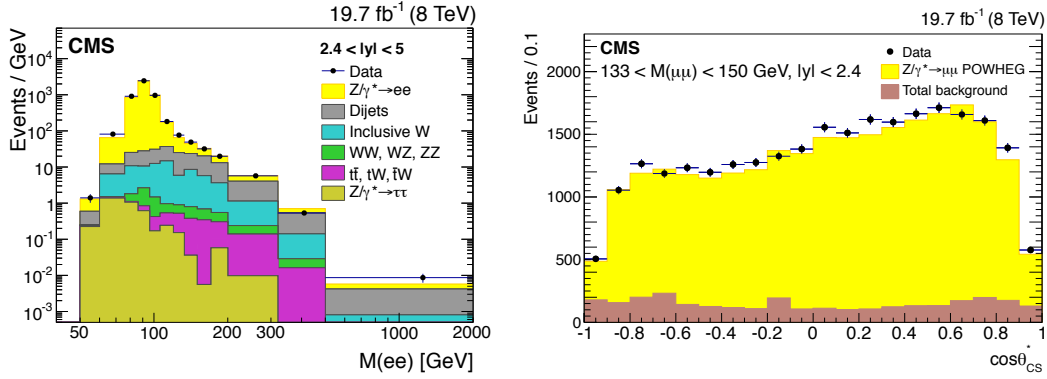


Figure 2: (left) The dilepton mass distributions for electron decay channels, for events with $2.4 < |y| < 5$. (right) A representative $\cos \theta_{CS}^*$ distribution for dimuon channel for $\mu\mu$ mass range 133 – 150 GeV [6].

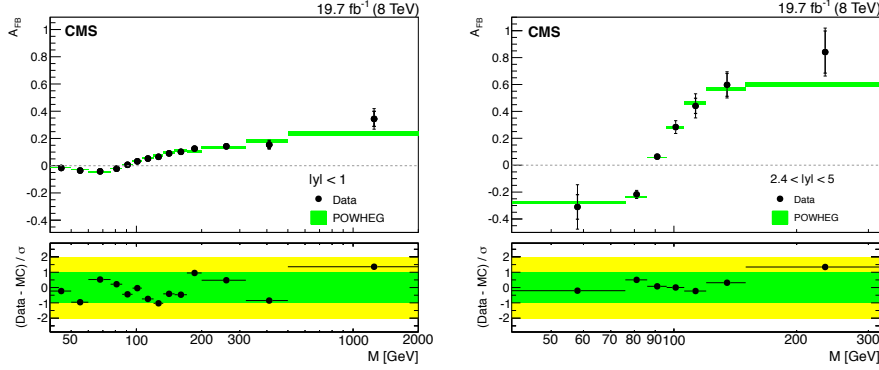


Figure 3: The combined dielectron and dimuon unfolded A_{FB} distributions in the central rapidity region $|y| < 1$ (left) and in the forward region for dielectron decay channel (right) [6].

and in the forward region for dielectron decay channel are shown in Fig. 3. The measured distributions agree well with the POWHEG predictions. Because A_{FB} in the forward rapidity region is less diluted, the measured A_{FB} quantity is closer to the parton-level asymmetry after the unfolding process, than it is in the central rapidity region.

3 Effective mixing angle measurements

Measurement of the backward-forward asymmetry can be used for extraction of the effective mixing angle. Such measurement was performed by all three experiments ATLAS [7], LHCb [8] and CMS [9], only recent LHCb result is discussed here in detail.

The LHCb potentially has higher power for measuring the effective mixing angle, than ATLAS and CMS, since it naturally collects events in the forward region, $2 < \eta < 5$. Figure 4 left shows the A_{FB} as a function of dimuon mass as measured in LHCb. Both muons are required to be within $2.0 < \eta < 4.5$ and have transverse momentum greater than 20 GeV. The measurements are performed with two data samples, at $\sqrt{s} = 7$ and 8 TeV, with luminosities of 1 and 2 fb⁻¹ respectively. The A_{FB} as a function of the dimuon invariant mass is compared with several sets of SM predictions generated with POWHEG for values of $\sin^2 \theta_W^{eff}$ ranging from 0.22 to 0.24. The Z-boson mass and electromagnetic coupling constant were fixed to their PDG values, NNPDF2.3 PDF set [10] was used with the strong coupling constant of 0.118. The agreement between data and predictions is quantified using χ^2 value, taking into account statistical, systematic and theoretical

uncertainties, and correlations between mass bins. A quadratic function is fitted to the χ^2 as shown in Fig. 4 right. The interval in $\sin^2 \theta_W^{eff}$ corresponding to variation of one unit in χ^2 is quoted as the uncertainty. Combination of 7 and 8 TeV results obtained by calculating the full covariance matrix for all uncertainties yields the value $\sin^2 \theta_W^{eff} = 0.23142 \pm 0.00073(stat) \pm 0.00052(sys) \pm 0.00056(theo)$.

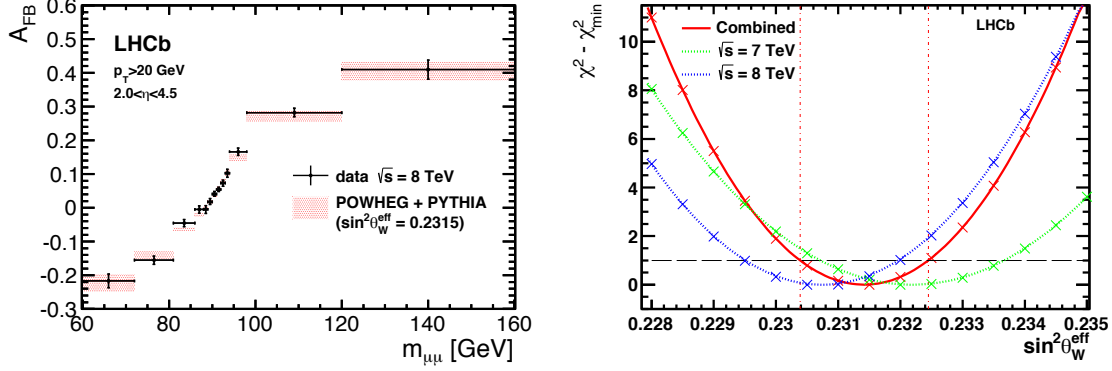


Figure 4: (Left) The A_{FB} as a function of the dimuon invariant mass. (Right) Difference between the χ^2 and the minimum χ^2 obtained by comparing the measured and predicted A_{FB} distribution for different values of $\sin^2 \theta_W^{eff}$ [8].

A comparison between the $\sin^2 \theta_W^{eff}$ results obtained by different experiments is shown in Fig. 5. The LHCb result agrees well with the world average and LHC results.

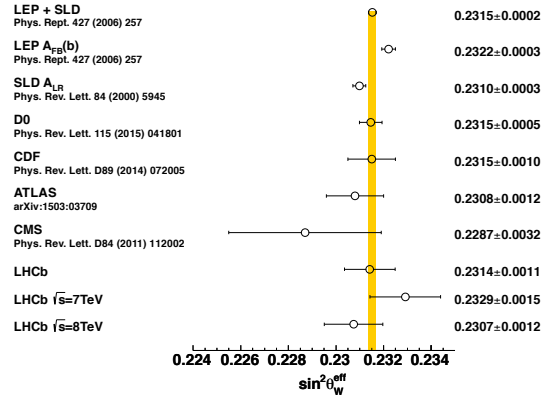


Figure 5: A comparison of the $\sin^2 \theta_W^{eff}$ measurement at LHCb and other experiments. The combined LEP and SLD measurement is indicated by the vertical yellow band [8].

4 Angular coefficients in Z-bosons events

The general structure of the lepton angular distribution in the boson rest frame is given by

$$\frac{d^2\sigma}{d\cos\theta^* d\phi^*} \propto \left[(1 + \cos^2\theta^*) + A_0 \frac{1}{2} (1 - 3\cos^2\theta^*) + A_1 \sin(2\theta^*) \cos\phi^* + A_2 \frac{1}{2} \sin^2\theta^* \cos(2\phi^*) + A_3 \sin\theta^* \cos\phi^* + A_4 \cos\theta^* + A_5 \sin^2\theta^* \sin(2\phi^*) + A_6 \sin(2\theta^*) \sin\phi^* + A_7 \sin\theta^* \sin\phi^* \right]. \quad (1)$$

where the θ^* is defined as in A_{FB} measurement, and ϕ^* is the azimuthal angle.

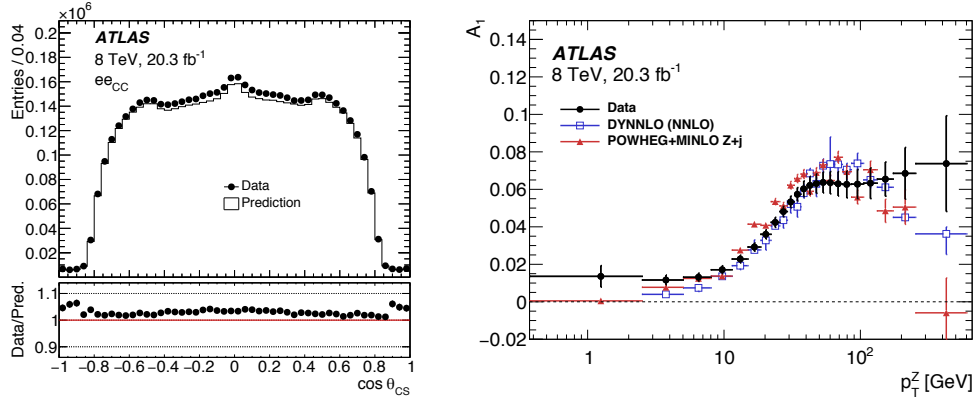


Figure 6: (Left) The $\cos \theta_{CS}$ angular distributions for dielectron channel. In the panel the ratios of the data to the summed signal+background predictions is shown, the uncertainty bars on the points only include those from data statistics. (Right) Distribution of the angular coefficient A_1 as a function of p_T^Z . The results are compared to the DNNLO and POWHEG MINLO predictions [12].

Parameters A_0 , A_1 , and A_2 are related to the polarization of the Z boson, whilst A_3 and A_4 are also sensitive to the V-A structure of the couplings of the leptons. All angular coefficients vanish as the Z boson transverse momentum approaches zero except for A_4 , which is the electroweak parity violation term. The Lam–Tung relation [11] $A_0 = A_2$ reflects the full transverse polarization of vector boson coupling to quarks, as well as rotational invariance. Processes containing non-planar configurations (e.g., from higher order multi-gluon emission) smear the transverse polarization, leading to $A_2 < A_0$. The A_5 , A_6 and A_7 coefficients appear first at NNLO in QCD.

In this section we discuss in detail only most recent ATLAS measurement [12] that was performed at 8 TeV for Z-bosons decaying to both electron and muon pairs with transverse momenta of the leptons above 25 GeV and for the Z-boson mass in the range 80–100 GeV.

The measurement of the angular coefficients is performed in multiple fine bins of p_T^Z and for a fixed dilepton mass window. Thus the data-simulation agreement in shape for these variables is less important, but it is important to verify qualitatively the level of agreement between data and MC simulation for the angular distributions, as shown in Fig. 6 left. The data and MC distributions are not normalized to each other, resulting in normalization differences at the level of a few percent. The measurement of the angular coefficients is, however, independent of this difference. The coefficients are extracted from the data by fitting templates to the reconstructed angular distributions. Each template is normalized by free parameters for its corresponding coefficient A_i , as well as an additional common parameter representing the unpolarised cross section. A likelihood is built from the nominal templates and the varied templates reflecting the systematic uncertainties. The muon and electron channels are combined through a likelihood multiplication.

Figure 6 (right) shows measured distribution of the angular coefficient A_1 as a function of p_T^Z compared to the DNNLO and POWHEG MINLO predictions. The NNLO predictions describe the data with some small discrepancy towards high p_T^Z values, still within uncertainties. Similar behavior was observed also for other coefficients. For the first time at the LHC the $A_5 - A_7$ coefficients are measured as shown in Fig. 7 left. As expected the Lam–Tung relation does not hold, but as one can see in Fig. 7 right the NNLO predicts much smaller deviation from 0 than observed in data. ATLAS results agree well with the previous CMS measurement [13], while extending it to measurement of the $A_5 - A_7$ coefficients.

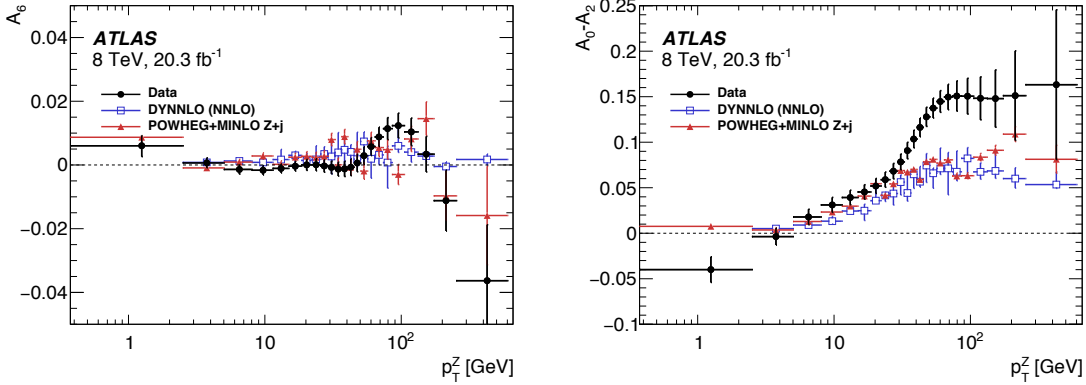


Figure 7: Distributions of the angular coefficients A_5 (left) and $A_0 - A_2$ (right) as a function of p_T^Z . The results from the measurements are compared to the DYNLO and POWHEG MINLO predictions [12].

5 Electroweak production of vector bosons in association with two jets

Electroweak production of vector bosons is characterized by production of one, in case of W production, or two, in case of Z, leptons in the central part of the detector with two jets in backward/forward directions separated by a large rapidity gap. The major background to EWK process is W/Z+jj QCD production. In the recent ATLAS Wjj analysis [14] for $\sqrt{s} = 7$ and 8 TeV, the electrons and muons are required to have $p_T > 25$ GeV, two jets with $p_T > 80(60)$ GeV, separated by $\Delta|y| > 2$, in presence of missing transverse energy (greater than 20 GeV) and transverse mass, $m_T > 40$ GeV. The signal region should contain only one lepton in the central region and no jets.

Predicted and observed distributions of the dijet invariant mass for events in the signal region is shown in Fig. 8 left. The measurement of the fiducial EWK Wjj cross section in the signal region is performed with an extended joint binned likelihood fit of the dijet mass distribution for the normalization factors of the QCD and EWK Powheg+Pythia8 predictions. The region at relatively low invariant mass 500–1000 GeV has low signal purity and primarily determines QCD contribution, while events with higher invariant mass have higher signal purity and mainly determine EWK contribution. The interference between the processes is not included in the fit, and is instead taken as an uncertainty based on SM predictions. The measured fiducial EWK cross sections $144 \pm 23(stat) \pm 23(exp) \pm 13(theo)$ fb for 7 TeV and $159 \pm 10(stat) \pm 17(exp) \pm 20(theo)$ fb for 8 TeV can be compared to predicted values of 144 ± 11 and 198 ± 12 fb for 7 and 8 TeV respectively. The paper also includes number of differential cross section measurements and set limits on anomalous triple-gauge-boson couplings. Figure 8 right demonstrates ratio of the measured to predicted values for different measurements of the cross section times branching fractions of electroweak production of a single W, Z, or Higgs boson at high dijet invariant mass for 7 and 8 TeV. Within uncertainties the measurements agree with predictions.

The above comparison does not yet include the first preliminary measurement of the EWK production of Z bosons at 13 TeV that was performed by CMS experiment [15]. The measurement requires pairs of electrons or muons, with mass within 15 GeV from the nominal Z-boson mass for leptons with $p_T > 30(20)$ GeV, leading(subleading) and two jets with $p_T > 50$ and 30 GeV. The dijet invariant mass for the dimuon channel is shown in Fig. 9 left. One can see that the EWK relative contribution increases with dijet mass as expected but still an order of magnitude less than the background QCD process even for very high masses. To improve the measurement a boosted decision tree (BDT) is used based on set of variables like the dijet pseudorapidity opening $\Delta\eta_{jj}$, the dijet transverse momentum and others. The BDT is trained to achieve the best separation between EWK and DY production and the results for dimuon channel are shown in Fig. 9 right. By comparing the left to the right plot, one can obviously see that, as expected, the BDT provides better separation between the signal and the background as the dijet mass distribution alone. The measured

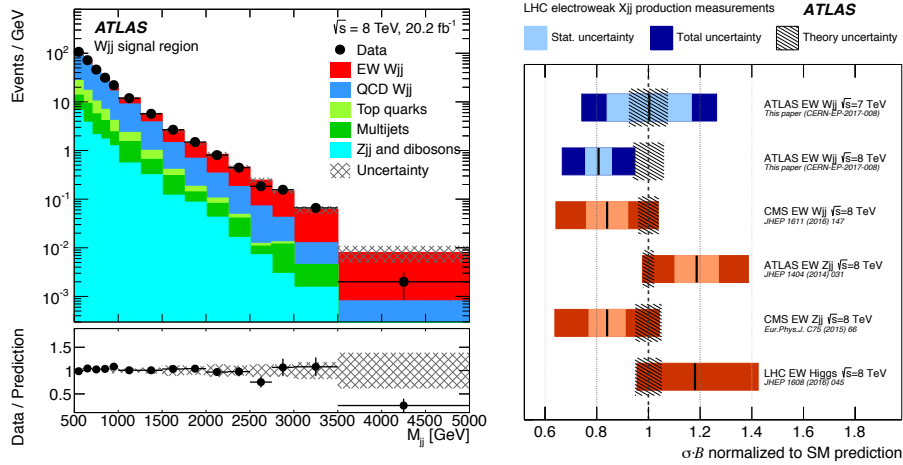


Figure 8: (Left) Distribution of the dijet invariant mass for events in the signal region in 8 TeV data, after fitting for the yields of the individual Wjj processes. The bottom panel shows the ratio of data to predicted signal-plus-background yields. The shaded band centred at unity represents the statistical and experimental uncertainties summed in quadrature. (Right) Measurements of the cross section times branching fractions of electroweak production of a single W, Z, or Higgs boson at high dijet invariant mass, divided by the SM predictions (Powheg+Pythia8 for ATLAS, Madgraph+Pythia8 for CMS, and Powheg+Pythia8 for the LHC combination). The lighter shaded band (where shown) represents the statistical uncertainty of the measurement, the outer darker band represents the total measurement uncertainty. Theoretical uncertainties in the SM prediction are represented by the shaded region centred at unity [14].

EWK cross section by combining electron and muon channels: $552 \pm 19(stat) \pm 55(syst)$ fb agrees well with the SM prediction, 543 ± 24 fb.

6 Summary

These proceedings present only some selected EWK measurements, there were more contributions presented at this conference that covered other EWK topics. The precise measurements require time to perform the data analyses and therefore we only now complete 7+8 TeV program and start to analyse 13 TeV data. In most of the cases the statistical uncertainties do not dominate the precision of the measurements and better understanding of systematics, and in some cases theoretical uncertainties, are required.

The University of Wisconsin Madison would like to acknowledge the U.S. Department of Energy (DOE) and the National Science Foundation (NSF) for funding their contribution to this research.

References

- [1] ATLAS Collaboration, JINST **3** S08003 (2008) .
- [2] LHCb Collaboration, JINST **3** S08005 (2008) .
- [3] LHCb Collaboration, Int. J. Mod. Phys. A **30** no.07, 1530022 (2015) .
- [4] CMS Collaboration, JINST **3** S08004 (2008) .
- [5] J. C.Collins and D. E.Soper, Phys. Rev. D **16**, 2219 (1977) .

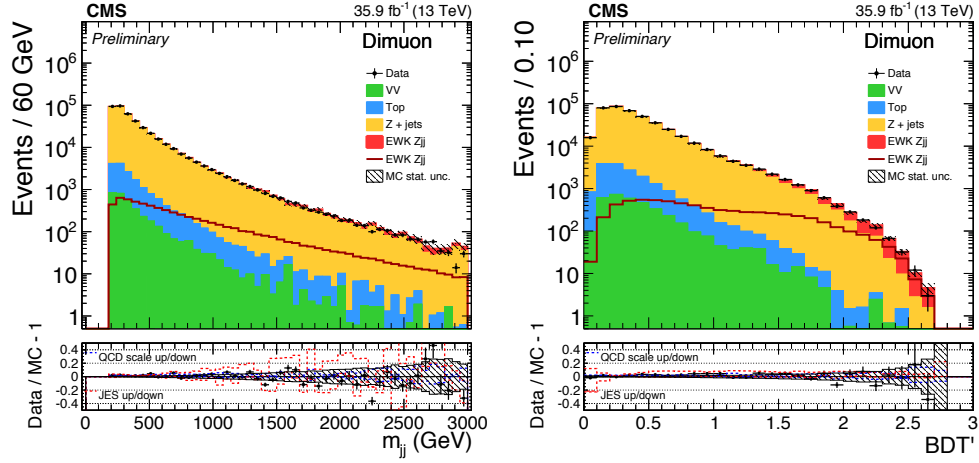


Figure 9: (Left) Invariant mass of the dijet system for data and simulated events. The contributions from the different background sources and the signal are shown stacked, with data points superimposed. The expected signal-only contribution is also shown as an unfilled histogram. The lower panel shows the relative difference between the data and expectations as well as the uncertainty envelopes for JES and QCD scales uncertainties. (Right) Distributions for the BDT discriminants in dimuon events [15].

- [6] CMS Collaboration, Eur. Phys. J. C **76**, no. 6, 325 (2016) .
- [7] ATLAS Collaboration, JHEP **09**, 049 (2015) .
- [8] LHCb Collaboration, JHEP **11**, 190 (2015) .
- [9] CMS Collaboration, Phys. Rev. D **84**, 112002 (2011) .
- [10] R.D. Ball *et al.* [NNPDF Collaboration], Nucl. Phys. B **867**, 244 (2013) .
- [11] C.S. Lam and Wu-Ki Tung, Phys. Lett. B **80**, 228 (1979).
- [12] ATLAS Collaboration, JHEP **08**, 159 (2016) .
- [13] CMS Collaboration, Phys. Lett. B **750** (2015) 154 .
- [14] ATLAS Collaboration, Eur. Phys. J. C **77** (2017) no.7, 474 .
- [15] CMS Collaboration, CMS-PAS-SMP-16-018, url. <https://cds.cern.ch/record/2261499> .